Published in final edited form as:
Brain Struct Funct. 2010 March ; 214(2-3): 145–160. doi:10.1007/s00429-010-0242-4.

Hippocampal interneuron loss in an APP/PS1 double mutant mouse and in Alzheimer's disease

Hisaaki Takahashi,
Department of Neuroscience, Maastricht University, 6200 MD Maastricht, The Netherlands. Department of Psychiatry and Neuropsychology, Maastricht University, 6200 MD Maastricht, The Netherlands. Department of Molecular and Cellular Physiology, Graduate School of Medicine, Ehime University, Matsuyama, Ehime 791-0295, Japan

Ivona Brasnjevic,
Department of Neuroscience, Maastricht University, 6200 MD Maastricht, The Netherlands. Department of Psychiatry and Neuropsychology, Maastricht University, 6200 MD Maastricht, The Netherlands. European Graduate School of Neuroscience (EURON), 6200 MD Maastricht, The Netherlands

Bart P. F. Rutten,
Department of Neuroscience, Maastricht University, 6200 MD Maastricht, The Netherlands. Department of Psychiatry and Neuropsychology, Maastricht University, 6200 MD Maastricht, The Netherlands. European Graduate School of Neuroscience (EURON), 6200 MD Maastricht, The Netherlands

Nicolien Van Der Kolk,
Department of Neuroscience, Maastricht University, 6200 MD Maastricht, The Netherlands. Department of Psychiatry and Neuropsychology, Maastricht University, 6200 MD Maastricht, The Netherlands. European Graduate School of Neuroscience (EURON), 6200 MD Maastricht, The Netherlands

Daniel P. Perl,
Department of Pathology (Neuropathology), Mount Sinai School of Medicine, New York, NY 10029, USA. Department of Neuroscience, Kastor Neurobiology of Aging Laboratories, Mount Sinai School of Medicine, 1 Gustave L. Levy Place, Box 1065, New York, NY 10029, USA

Constantin Bouras,
Department of Psychiatry, University of Geneva School of Medicine, 1225 Geneva, Switzerland. Department of Neuroscience, Kastor Neurobiology of Aging Laboratories, Mount Sinai School of Medicine, 1 Gustave L. Levy Place, Box 1065, New York, NY 10029, USA

Harry W. M. Steinbusch,
Department of Neuroscience, Maastricht University, 6200 MD Maastricht, The Netherlands. Department of Psychiatry and Neuropsychology, Maastricht University, 6200 MD Maastricht, The Netherlands. European Graduate School of Neuroscience (EURON), 6200 MD Maastricht, The Netherlands

Christoph Schmitz,
Department of Neuroscience, Maastricht University, 6200 MD Maastricht, The Netherlands. Department of Psychiatry and Neuropsychology, Maastricht University, 6200 MD Maastricht, The Netherlands. European Graduate School of Neuroscience (EURON), 6200 MD Maastricht, The

Correspondence to: Dara L. Dickstein, dara.dickstein@mssm.edu.
H. Takahashi and I. Brasnjevic contributed equally to this study.

Netherlands. Department of Neuroscience, Kastor Neurobiology of Aging Laboratories, Mount Sinai School of Medicine, 1 Gustave L. Levy Place, Box 1065, New York, NY 10029, USA

Patrick R. Hof, and
Department of Neuroscience, Kastor Neurobiology of Aging Laboratories, Mount Sinai School of Medicine, 1 Gustave L. Levy Place, Box 1065, New York, NY 10029, USA

Dara L. Dickstein
Department of Neuroscience, Kastor Neurobiology of Aging Laboratories, Mount Sinai School of Medicine, 1 Gustave L. Levy Place, Box 1065, New York, NY 10029, USA

Dara L. Dickstein: dara.dickstein@mssm.edu

Abstract

Hippocampal atrophy and neuron loss are commonly found in Alzheimer's disease (AD). However, the underlying molecular mechanisms and the fate in the AD hippocampus of subpopulations of interneurons that express the calcium-binding proteins parvalbumin (PV) and calretinin (CR) has not yet been properly assessed. Using quantitative stereologic methods, we analyzed the regional pattern of age-related loss of PV- and CR-immunoreactive (ir) neurons in the hippocampus of mice that carry M233T/L235P knocked-in mutations in presenilin-1 (PS1) and overexpress a mutated human beta-amyloid precursor protein (APP), namely, the APP^{SL}/PS1 KI mice, as well as in APP^{SL} mice and PS1 KI mice. We found a loss of PV-ir neurons (40–50%) in the CA1-2, and a loss of CR-ir neurons (37–52%) in the dentate gyrus and hilus of APP^{SL}/PS1 KI mice. Interestingly, comparable PV- and CR-ir neuron losses were observed in the dentate gyrus of postmortem brain specimens obtained from patients with AD. The loss of these interneurons in AD may have substantial functional repercussions on local inhibitory processes in the hippocampus.

Keywords

Alzheimer's disease; Amyloid precursor protein; Calcium-binding proteins; Hippocampus; Presenilin-1; Stereology

Introduction

Alzheimer's disease (AD) is characterized neuropathologically by extracellular aggregates of amyloid beta protein (Aβ) derived from the amyloid precursor protein (APP), intracellular neurofibrillary tangles, and synapse and neuron loss (Cummings and Cole 2002). In addition, most neurotransmitter systems show alterations in AD (Gsell et al. 2004). Deficits in GABAergic transmission seem to play an important role in the cognitive and behavioral symptoms of AD (Gsell et al. 2004; Lanctot et al. 2004). In the hippocampus, which is severely affected in AD (Cummings and Cole 2002; Hof and Morrison 2004), inhibition is mediated by largely non-overlapping subsets of GABAergic interneurons that can be identified by the presence of the calcium-binding proteins parvalbumin (PV), calretinin (CR), and calbindin (CB) (Freund and Buzsaki 1996; Maccaferri and Lacaille 2003). These proteins can be used as markers of selective neuronal degeneration (Hof et al. 1991, 1993) since depletion of calcium-binding proteins deprives neurons the ability to maintain intracellular calcium levels and renders them vulnerable to pathological processes (Popovic et al. 2008). Several neuropathologic studies have addressed the status of PV-, CR-, and CB-immunoreactive (ir) neurons in the brains of AD patients. However, these studies have yielded conflicting results and only few reported on the hippocampus. In particular, it is not known whether hippocampal CR-ir neurons are affected in AD.

We recently demonstrated an age-related loss of neurons of approximately 50% in the CA1-2 region of the hippocampus in 10-month-old APP^{SL}/PS1ho KI mice (Casas et al. 2004). These mice express the human mutant APP carrying the Swedish (K670N/M671L) and London (V717I) mutations under control of the Thy1 promoter, and the human presenilin (PS) 1 mutations M233T and L235P knocked-in into the mouse PS1 gene in a homozygous manner (Casas et al. 2004). In the present study, we investigated whether subpopulations of hippocampal PV- and CR-ir neurons are regionally and selectively affected in the hippocampus of APP^{SL}/PS1ho KI mice, and examined the degree to which the loss of these GABAergic interneurons parallels the overall neuron loss in the same mice. To explore the specific roles of mutant APP and mutant PS1 in age-related neuron loss in this mouse model of AD, we also investigated APP^{SL} mice that express the human mutant APP carrying the Swedish and London mutations, as well as PS1he KI mice and PS1ho KI mice that express the human PS1 mutations M233T and L235P knocked-in into the mouse PS1 gene in a hemizygous or homozygous manner, respectively. In addition, we investigated the status of PV- and CR-ir neurons in the dentate gyrus and hilus of the hippocampus in postmortem brains from AD patients and age-matched controls. As the morphology, distribution, and local connectivity of distinct subsets of GABAergic interneurons differs, identifying deficits of specific cortical interneurons in AD could help identifying possible mechanisms underlying the disturbances of hippocampal function observed in this disease.

Materials and methods

Animals and human postmortem tissue

The following groups of 2-month-old (M2) and 10-month-old (M10) mice were investigated: (1) APP^{SL} mice [M2: $n = 3$ (1 female and 2 males); M10: $n = 6$ (2 females and 4 males)]; (2) PS1he KI mice [M2: $n = 4$ (2 females and 2 males); M10: $n = 6$ (4 females and 2 males)]; (3) PS1ho KI mice [M2: $n = 5$ (1 female and 4 males); M10: $n = 4$ (4 males)]; and (4) APP^{SL}/PS1ho KI mice [M2: $n = 4$ (2 females and 2 males); M10: $n = 4$ (2 females and 2 males)]. A detailed description of these transgenic/knocked-in mice was previously published (Casas et al. 2004). All experiments were performed in compliance with the German animal protection law, considering international standards and NIH recommendations.

Brains from ten patients presenting with AD (86.4 ± 2.2 years; mean ± SEM) and ten patients with no history of neurologic or psychiatric disorders (84.6 ± 2.8 years) were obtained at autopsy from the Alzheimer's Disease Research Center Brain Bank, Mount Sinai School of Medicine (New York, NY, USA) and the Department of Psychiatry, University of Geneva School of Medicine (Geneva, Switzerland) (Table 1). The postmortem delays ranged from 2 to 6 h. The clinical dementia rating (CDR) scores were ascertained as described previously (Morris 1993). Dementia was rated on a scale from 0 to 5 (CDR 0, no dementia; CDR 0.5, very mild; CDR 1, mild; CDR 2, moderate; CDR 3, severe; CDR 4, profound; and CDR 5, terminal dementia). AD was neuropathologically confirmed by the presence of large numbers of neurofibrillary tangles and amyloid deposition in the hippocampal formation and the neocortex. The assessment of neurofibrillary pathology followed the staging recommended by Braak and Braak (1991). In the control cases, isolated neurofibrillary tangles were occasionally observed only in the hippocampal formation. There was no evidence of traumatic lesions, infections, gross area of infarction, primary tumor, or metastatic process in any of the AD or control brains. All protocols involving human postmortem materials were approved by the relevant Institutional Review Boards and ethics committee.

Tissue processing

Mice were anesthetized and transcardially perfused as previously described (Schmitz et al. 2004). The brains were rapidly removed from the skulls and halved in the mediosagittal line. The left brain halves were cryoprotected by immersion in 30% sucrose, quickly frozen and cut into entire series of 30-μm-thick coronal sections. These series of sections were then divided into subseries of every tenth section, yielding ten series of 5–8 sections containing the hippocampus in each animal.

One subseries of every tenth section of the left brain half per animal was mounted on glass slides, dried, defatted with Triton X-100 (0.025%, 20 min; Merck, Darmstadt, Germany) and stained with cresyl violet (0.01%, 15 min).

A second subseries of every tenth section of the left hemisphere from each animal was used for immunohistochemical detection and quantification of Aβ and glial fibrillary acidic protein (GFAP) as recently described (Schmitz et al. 2004). Immunohistochemistry on free-floating sections was performed using standard immunofluorescence labeling procedures. Briefly, sections were washed 3 × 15 min in 0.1 M Tris-buffered saline (TBS, pH 7.6), with the addition of 0.3% Triton X-100 (TBS-T), preincubated at room temperature (20°C). Sections were then treated with 10% fetal calf serum and 4% non-fat dry milk in TBS, to block non-specific binding sites, and then incubated overnight at 4°C in the following primary antibodies: monoclonal mouse anti-GFAP IgG1 clone G-A-5 (Sigma, St. Louis, MO, USA; catalog #G3893; dilution 1:1,600) raised against purified GFAP from pig spinal cord and rabbit anti-mouse polyclonal antiserum 730 (against human Aβ and P3; generously provided by Gerd Multhaup; Borchardt et al. 1999; Wirths et al. 2002, dilution 1:1,500) raised against a synthetic peptide corresponding to human Aβ residues 1–40. Following incubation in primary antibody, the sections were rinsed 3 × 15 min in TBS and incubated with secondary antibodies for 1.5 h at room temperature. Donkey anti-mouse IgG Alexa Fluor 488 (1:100; Molecular Probes, Eugene, OR, USA) and donkey anti-rabbit IgG Alexa Fluor 594 (1:100; Molecular Probes) were used as secondary antibodies. Sections were washed, counterstained with Hoechst 33342 (1:500; Sigma), mounted on glass slides and coverslipped with 80% glycerol-TBS. The expected cellular morphology and distribution of staining for each primary antibody were consistent with earlier studies.

A third subseries of every tenth section of the left hemisphere from each animal was used for immunofluorescent detection of parvalbumin (PV) and calretinin (CR) (three free-floating sections per animal, representing approximately Bregma coordinates −1.22, −1.94, and −3.08 according to Franklin and Paxinos 1997). For PV, a mouse monoclonal IgG1 clone parv-19 (Sigma, catalog #P3088, 1:8,000) raised against purified frog muscle PV was used which specifically recognizes PV in a calcium-dependent manner at 12 kDa on immunoblot (manufacturer's datasheets). For detecting CR, a mouse monoclonal clone 6B3 (Swant, catalog #6B3, 1:2,000) raised against recombinant human CR-22K, was used. Briefly, free-floating sections were washed 3 × 15 min in 0.1 M TBS (pH 7.6), with the addition of 0.3% Triton X-100, preincubated at room temperature (20°C). After this, sections were incubated in monoclonal mouse anti-PV antibody solution and polyclonal rabbit anti-mouse anti-CR antibody solution (antibodies descriptions stated above) in TBS-T for overnight at 4°C. Following incubation, the sections were washed 3 × 15 min in TBS, and incubated at room temperature for 2 h in the secondary antibodies (donkey anti-mouse IgG Alexa Fluor 488; 1:200 and donkey anti-rabbit IgG Alexa Fluor 594; 1:200, Molecular Probes). After an additional set of three washes in TBS, sections were counterstained with Hoechst 33342 (1:500; Sigma) for 10 min at room temperature and immediately thereafter mounted on glass and coverslipped with 80% glycerol-TBS.

Finally, a fourth subseries of every tenth section of the left hemisphere from each APP^{SL} mice and APP^{SL}/PS1ho KI mice was incubated with thioflavin S (1%; Sigma) according to a standard protocol (Schmidt et al. 1995). Briefly, sections were immersed in 0.05% $KMnO_4$ in PBS for 20 min. After rinsing in phosphate buffered saline (PBS), the sections were destained in 0.2% $K_2S_20_5$ and 0.2% oxalic acid in PBS for 3 min in the dark. After rinsing in PBS, sections were incubated in a 0.0125% solution of thioflavin S in 40% ethanol and 60% PBS. Finally, the sections were differentiated in 50% ethanol in PBS, rinsed in PBS, counterstained with Hoechst 33342 (1:500; Sigma), and mounted as above.

The tissue blocks from the human brains were cut serially in 50-μm-thick sections on a Vibratome (Leica, Vienna, Austria). Immunohistochemistry was performed on free-floating sections with a rabbit anti-CR polyclonal antibody (Swant, catalog #7699/4, 1:3,000) raised against recombinant human CR, which does not cross-react with other closely related calcium-binding proteins such as calbindin D-28K (manufacturer's datasheets; Schwaller et al. 1993). Sections stained for CR were treated as previously described (Nimchinsky et al. 1997). Vibratome sections were pretreated with 30% H_2O_2 for 10 min, rinsed, and preincubated in normal goat serum (NGS, 1:5) for 45 min. After incubation overnight with primary antibody, detection was performed using biotinylated goat anti-mouse IgGs (1:200, 30 min, Dako, Glostrup, Denmark) and an avidin–biotin horseradish peroxidase solution (Vectastain Elite ABC, Vector Laboratories, Burlingame, CA) and 3,3′-diaminobenzidine (DAB) as a chromogen, intensified in 0.005% osmium tetroxide. All incubations and rinses (3 × 10 min) were performed at room temperature under gentle agitation in TBS-T (0.01 M Tris, 0.9% NaCl, 0.3% Triton-X 100, pH 7.6). Sections stained for PV were processed as above but stained with a modified glucose oxidase and nickel-ammonium sulfate-intensified DAB method (Shu et al. 1988; Van Der Gucht et al. 2006). All sections were mounted on 2% gelatin-subbed slides, counterstained with cresyl violet, and coverslipped using DPX (Sigma).

Stereologic analyses

Stereologic analyses were performed with a computer-based stereology workstation, consisting of a modified light microscope [Olympus BX50 with UPlanApo objectives 10× (NA = 0.4), 20× (oil; NA = 0.7), 40× (oil; NA = 1.0) and 100× (oil; NA = 1.35); Olympus, Tokyo, Japan], a motorized specimen stage for automatic sampling (Ludl Electronics, Hawthorne, NY, USA), a focus drive linear encoder (Ludl Electronics), a CCD color video camera (HV-C20AMP; Hitachi, Tokyo, Japan), and stereology software (StereoInvestigator v. 7.00.03; MBF Bioscience, Williston, VT, USA).

The sections from the left mouse brain hemispheres stained with cresyl violet were used to estimate the volumes of the following regions in the hippocampus with the Cavalieri's principle (as shown in Fig. 2 in Schmitz and Hof 2005): dentate gyrus [stratum granulare, hilus, and stratum moleculare (SM) analyzed separately], area CA3 [stratum pyramidale (SP), stratum oriens (CA3-OR), and stratum lucidum (SL) analyzed separately] and area CA1-2 [stratum pyramidale, stratum oriens (CA1-2-OR) and stratum radiatum (SR) analyzed separately]. In all analyses, a deliberate choice was made to group the CA1 and CA2 together to match the design of previous studies in these transgenic models (Casas et al. 2004; Rutten et al. 2005; Schmitz et al. 2004). Estimates were performed with a 10× objective by tracing the boundaries of these regions on all sections in which they were found on video images displayed on the computer screen, and multiplying the sum of all cross-sectional areas of a given region with a uniform distance between the sections (i.e., 10 × 30 μm). Data from the hilus, SM, CA3-OR, SL, CA1-2-or and SR were combined into estimates of the volume of the white matter of the hippocampus.

The sections from the left mouse brain hemispheres processed for the detection of PV and CR were used to determine the densities of PV- and CR-ir neurons in all regions of the hippocampus mentioned above. Due to the location of many PV- and CR-ir neurons at the border between the stratum granulare in the dentate gyrus and the hilus, these regions were analyzed together. SM, CA3-or, SL, CA1-2-or and SR were also analyzed together because of the low numbers of PV- and CR-ir neurons in the different parts of the white matter of the hippocampus. All PV- and CR-ir neurons which came into focus within the section thickness of all sections immunoprocessed for the detection of PV and CR were counted with the 20× objective in the different regions of the hippocampus. Then, densities of PV- and CR-ir neurons were calculated by dividing the numbers of counted PV- and CR-ir neurons per region by the product of the sum of all cross-sectional areas of this region (analyzed with the Hoechst counter-staining) with the section thickness (30 μm). Total numbers of PV- and CR-ir neurons were obtained by multiplying the densities of PV- and CR-ir neurons with the volumes of the corresponding regions in the hippocampus obtained on the sections stained with cresyl violet.

Finally, the sections from the left hemispheres processed for the detection of Aβ and GFAP as well as the sections incubated with thioflavin S were used to assess the deposition of extracellular Aβ aggregates in the different regions of the hippocampus.

On the sections from the human brains, densities of PV-and CR-ir neurons were determined by counting all PV- or CR-ir neurons in the stratum granulare in the dentate gyrus and the hilus with a 20× objective which came into focus within the section thickness of all sections immunoprocessed for the detection of PV and CR (5–8 sections per brain). Then the number of counted PV- and CR-ir neurons were divided by the product of the sum of all cross-sectional areas of the stratum granulare in the dentate gyrus and the hilus (analyzed on the cresyl violet counterstaining) and the section thickness (50 μm). Because the available tissue blocks from the human brains did not represent the entire length of the hippocampus, it was not possible to estimate total numbers of PV- or CR-ir neurons.

Photography

Photomicrographs were produced by digital photography using an Olympus DP 70 digital camera attached to an Olympus AX 70 microscope and cell^{P} software (v. 2.3; Soft Imaging System, Münster, Germany; Figs 2, 3, 4, and 6), or using a Hamamatsu C9100-02 digital camera (Hamamatsu Photonics, Hamamatsu City, Japan) attached to a StereoInvestigator Confocal Spinning Disk system (MBF Bioscience). Photomicrographs shown in Figs. 2, 3, 4, and 6 were prepared with Imaris software (v. 4.0.3; Bitplane, Zurich, Switzerland). The final figures were constructed using Corel Photo-Paint v.11 and Corel Draw v.11 (Corel, Ottawa, Canada). Only minor adjustments of contrast and brightness were made, without altering the appearance of the original materials.

Statistical analysis

For all groups of mice, means and standard error of the mean (SEM) were calculated for all investigated variables. Comparisons between the groups were performed using generalized linear model univariate analysis of variance, with age and genotype as fixed factors and the animals' sex as covariate. When statistically significant ($p \leq 0.05$) differences were found in the ANOVA calculations, data from the 2-month-old animals were compared with the corresponding data from the 10-month-old animals of the same genotype with a Bonferroni test. For human studies, comparison between two groups was performed using generalized linear model univariate analysis of variance, with diagnosis (i.e., control vs. AD based on CDR score) as fixed factors and the patients' gender and age as covariates. In all analyses an effect was considered statistically significant if its associated p value was smaller than 0.05.

Calculations were performed using SPSS (v. 12.0.1 for Windows; SPSS, Chicago, IL, USA). Graphs were constructed using GraphPad Prism (v. 4.00 for Windows; GraphPad Software, San Diego, CA, USA).

Results

Age-related reductions in hippocampus volume of PS1ho KI and APP^{SL}/PS1ho KI mice

Significant age-related reductions in volumes of hippocampal subfields between M2 and M10 were found in PS1ho KI mice [stratum granulare in the dentate gyrus (DG-SG): −23.3%, $p = 0.002$; stratum pyramidale in the CA1-2 (CA1-2-SP): −29.8%; $p = 0.01$], and particularly in APP^{SL}/PS1ho KI mice (CA1-2-SP: −48.4%, $p = 0.01$; white matter: −17.5%, $p = 0.036$; Table 2). Trend-level differences that did not reach statistical significance owing to the biological variability, but not the accuracy, of the volumetric estimates, were observed in the DG and CA3 of the APP^{SL}/PS1ho KI and PS1he KI mice. This loss of volume can be attributed to neuronal loss as previously reported for CA1-2 by Casas et al. (2004).

Age-related accumulation of amyloid deposits and activated astrocytes in the hippocampus of PS1ho KI and APP^{SL}/PS1ho KI mice

Staining with antibodies that recognize Aβ and P3, glial fibrillary acidic protein (GFAP), and staining with Hoechst 33342 shows the presence of extracellular Aβ aggregates and surrounding astrocytes in APP^{SL} mice and APP^{SL}/PS1ho KI mice (Fig. 2). The presence of Aβ deposits exhibits an age-related effect with more aggregates and stronger GFAP immunoreactivity present in the brains of M10 compared to M2 particularly in the CA1-2 region.

Age-related reductions in mean numbers of PV-ir neurons and CR-ir neurons in the hippocampus of PS1he KI, PS1ho KI, and APP^{SL}/PS1ho KI mice

Significant age-related reductions in the numbers of PV-ir neurons between M2 and M10 were found in CA1-2-SP of PS1he KI mice (−43.8%; $p < 0.05$), PS1ho KI mice (−49.4%, $p < 0.05$), and APP^{SL}/PS1ho KI mice (−42.7%; $p < 0.05$) (Figs. 1, 3, 4; Tables 2, 3). In contrast, age-related reductions in the numbers of CR-ir neurons were found in DG-SG and hilus of PS1ho KI mice (−37.8%; $p < 0.01$) and APP^{SL}/PS1ho KI mice (−51.6%; $p < 0.05$; Figs. 1, 3, 4; Tables 2, 3). This loss of PV- and CR-ir neurons could not be explained by the local presence of extracellular Aβ aggregates and surrounding astrocytes and may be due to the presence of the mutated PS1 gene (Fig. 2). Furthermore, in the DG-SG and hilus of APP^{SL}/PS1ho KI mice, the density of CR-ir neurons was significantly decreased between M2 and M10 (−49.3%; $p = 0.006$; Fig. 5; Tables 2, 3).

Distribution and pathology of PV- and CR-ir neurons in the dentate gyrus and hilus in AD

The pattern of PV and CR immunostaining in the human DG-SG and hilus has been described previously and therefore we provide only a brief description here (see Table 4 for references and Fig. 6 for typical patterns). CR immunostaining identifies a subpopulation of interneurons that are mainly distributed in the hilar region of the dentate gyrus, whereas neurons in the stratum granulare are scarcely immunostained (Fig. 6). As for PV-ir neurons, they are mainly located within or close to the stratum granulare of the dentate gyrus (Fig. 6). Generalized linear model univariate analysis of variance revealed no differences in density of PV-ir neurons in DG-SG and hilus of the hippocampus between AD and control cases ($p = 0.435$; Table 2; Fig. 7a) In contrast, a dramatic reduction in the mean densities of CR-ir neurons within the same region was observed in AD patients compared to controls (−63.2%; $p = 0.001$; Table 2; Fig. 7b).

Discussion

Summary of results

The principal finding of the present study is a previously unreported pattern of regionally specific age-related loss of PV- and CR-ir neurons within the hippocampus of a transgenic/knock-in mouse model of AD, APP^{SL}PS1KI, which carries two APP FAD-linked mutations and two PS1 knock-in mutations. This loss of interneurons is accompanied by a reduction in pyramidal cells in the CA1-2 in the same mice (Casas et al. 2004; Brasnjevic et al. submitted). The region-specific reduction in the number of PV-ir neurons in the CA1-2 of the APP^{SL}/PS1ho KI mice paralleled the intracellular accumulation of Aβ in neurons in this area and was in line with previous reports of neuron loss in postmortem brains from AD patients (Brady and Mufson 1997; West et al. 1994). However, this similarity should be taken cautiously because the results in the mouse brains could have been caused by the preferential expression of the Thy1 promoter in the CA1-2 in the transgenic constructs. We also observed a notable selective reduction in the density of GABAergic interneurons containing CR in DG-SG and the hilus of the hippocampus in brains from AD patients compared to controls lending support to our findings in these mouse models that different GABAergic local circuit neurons are selectively affected in the hippocampus. It is interesting in this context that the selective hippocampal pathology found in APP^{SL}/PS1ho KI mice bears an apparent similarity to autopsy findings in AD patients compared to age-matched controls. It should nonetheless be kept in mind that, as for any such animal model, caution should be exercised when relating murine APP/PS1 phenotype to human late-onset AD, most of which occurs in the absence of either APP or PS1 mutations.

Characterization of APP^{SL}/PS1ho KI mice

Other studies using mouse models overexpressing familial AD (FAD)-linked APP and/or PS1 mutations failed to demonstrate either pure intraneuronal Aβ deposition or considerable neuronal loss by quantitative neuron counting methods (Calhoun et al. 1998; Dickson 2004; Howlett et al. 2008; Irizarry et al. 1997; Takeuchi et al. 2000; Van Broeck et al. 2008), with the exception of one study describing loss of granule cells in the hippocampus of APP^{SL}/PS1ho KI mice (Cotel et al. 2008). It is worth noting that we used M10 animals whereas Cotel et al. (2008) analyzed M12 animals, and that in this transgenic mouse model a dramatic loss of neurons between 10 and 12 months of age cannot be excluded. Also, these authors investigated only female animals, whereas we investigated male and female animals, and as such, a specific sex effect cannot be excluded either. However, inconsistencies between the findings of Cotel et al. (2008) and the existing literature with respect to the volume estimates in transgenic mouse models of AD (e.g., (Casas et al. 2004; Rutten et al. 2003; Schmitz et al. 2004) were not discussed by these authors.

Methodologically, it should be noted that the relative densities of PV- and CR-ir neurons in the various subfields of the hippocampus in the mouse brains at M2 found in the present study were similar to those in previous reports (Bonthius et al. 2004; Casas et al. 2004; Nomura et al. 1997; Rutten et al. 2003). Finally, the groups of normal controls in our study showed almost the same ratio of CR-ir/PV-ir neurons in the DG as that reported by Zhang and Reynolds (2002) [the absolute numbers cannot be compared directly to each other because we expressed densities as number of neurons per mm^3 (i.e., volume) whereas Zhang and Reynolds as number of neurons per mm^2 (i.e., area)].

Differential vulnerability of PV-ir neurons and CR-ir neurons in hippocampus of PS1he KI, PS1ho KI, and APP^{SL}/PS1ho KI mice, and in AD

PV-ir neurons in the hippocampus correspond to basket or chandelier cells (reviewed in Freund and Buzsaki 1996), make contacts on somata and axonal initial segments of

pyramidal neurons in the CA3 and CA1-2 to regulate pyramidal cells output, and play a critical role in working and episodic memory (Fuchs et al. 2007). A subset of these cells shows a specific pattern of subunits of the α-amino-3-hydroxy-5-methyl-4-isoxazole-propionic acid (AMPA) receptors, with intense GluR3 immunoreactivity and no GluR2 immunoreactivity (Moga et al. 2003). This expression pattern of AMPA receptor subunits has been hypothesized to make these interneurons selectively vulnerable to excitotoxicity (Moga et al. 2003). With respect to the CR-ir neurons, two types can be distinguished in the hippocampus on the basis of dendritic morphology and distribution. The spine-free CR-ir neurons have 2–5 primary dendrites arising from their multipolar, bipolar or fusiform cell bodies, and can be found in all areas and layers of the hippocampus, showing a rather homogeneous distribution (Gulyas et al. 1996). These neurons seem to play a crucial role in the generation of synchronous, rhythmic hippocampal activity by controlling other interneurons terminating on different dendritic and somatic compartments of the principal cells (Gulyas et al. 1996). In contrast, the spiny CR-ir neurons are mostly present in the hilus of the dentate gyrus and in the stratum lucidum of the CA3 (Freund and Buzsaki 1996; Gulyas et al. 1996). These cells are covered with long, often branching spines, and their axons arborize in the stratum lacunosum-moleculare of the CA3 (Freund and Buzsaki 1996). The spiny CR-ir neurons (as well as PV- and substance P-receptor-ir neurons in the hilus) are innervated by mossy fibers via small en passant synapses or filopodial terminals (Acsady et al. 1998). Interestingly, in ischemia the spiny CR-ir neurons in the hilus of the dentate gyrus are the most vulnerable cells in the hippocampus (Freund and Magloczky 1993). Although no distinction could be made in the present study between spine-free and spiny CR-ir neurons on the basis of dendritic morphology, the specific distribution of these cells in the hippocampus suggests that particularly the spiny CR-ir neurons were lost during aging in the hippocampus of the PS1ho KI mice and the APP^{SL}/PS1ho KI mice as well as in human AD. The loss (Lazarov et al. 2006; Palop et al. 2003; Popovic et al. 2008) or preservation (Lee et al. 2004) of subsets of GABAergic interneurons expressing calcium-binding proteins has been shown also in some other AD animal models. Some of these studies, particularly a recent analysis in mice carrying both human $APP695_{swe}$ mutation and PS1 A246E mutation (Popovic et al. 2008), provide evidence for differential vulnerability of PV- and CR-ir neurons in the dentate gyrus in transgenic mice versus non-transgenic mice. These data are in agreement with the present results demonstrating that the vulnerability of calcium-binding neurons in transgenic mice is subregion-specific. Thus far, however, aging effects on subregion-specific changes in calcium-binding proteins in the hippocampus of these mice have not been investigated. The particular molecular mechanisms of leading to the death of PV- and CR-ir neurons in these mice will require further investigation, as well as the repercussion of their loss on the intrinsic connectivity of the hippocampal formation.

Functional implications of age-related loss of PV- and CR-ir neurons

Clearly the loss of PV and CR immunoreactivity does not necessarily imply the death of cells that normally contain these calcium-binding proteins. In animal models of epilepsy, the transient cessation of PV and CR synthesis, or an alteration of the conformation of PV and CR due to calcium overload, were proposed as possible causes of the decreased immunostaining (Dominguez et al. 2003; Scotti et al. 1997). Similar mechanisms might operate in animal models of AD and in human AD as well.

Regardless of the reason for the lower numbers of PV- and CR-ir neurons, it is important to bear in mind that altered levels of these proteins could perturb normal function of the hippocampus. We propose that loss of (spiny) CR-ir neurons in the hilus of the DG of both mice and AD cases would lead to a reduced inhibition of granule cells, which in turn may strengthen the excitatory projections from the DG to CA3 pyramidal cells. Similarly, specific dysfunction of PV-ir neurons showing high GluR3 immunoreactivity and lack of

GluR2 immunoreactivity (Moga et al. 2003) may have significant repercussions on the activity of the principal neurons in the CA1-2. Two studies showing the presence of dystrophic CR-ir neurites in the parahippocampal gyrus and subiculum in postmortem brains from AD patients (Brion and Résibois 1994) as well as decline of CR immunoreactivity in the innermost part of the molecular layer of the DG (Kaufmann et al. 1998; Selke et al. 2006) fit well with aberrant mossy fiber sprouting. Loss of PV-ir and other GABAergic interneurons, as well as hippocampal hyperexcitability has been observed in AD and other neurological disorders (Bazzett et al. 1994; Brady and Mufson 1997; Selke et al. 2006). In this context, it must be kept in mind that the present study was limited to PV and CR as marker of GABAergic neurons, which in no manner is meant to be representative of the complex neurochemical phenotype of these neurons (Freund and Buzsaki 1996). Our study was indeed limited by the availability of animals and the number of markers that we could include altogether in a rather complicated stereologic design. Future studies, involving additional markers, such as the calcium-binding protein calbindin and neuropeptides such as somatostatin, are necessary to assess further the significance of specific changes in GABAergic cell subtypes in the hippocampal subfields in AD.

PS1-driven age-related loss of PV- and CR-ir neurons

Detailed stereologic analyses of APP^{SL} mice revealed no disease-specific pathology. Although the possibility that the effect would be observed at older time-points, the lack of decrease in numbers of PV- and CR-ir neurons in the hippocampus of APP^{SL} mice at M10, indicate that mutations in APP are not necessary for such reductions to occur in APP^{SL}/PS1ho KI mice. As to why human mutant PS1 can cause age-related loss of PV-ir neurons in the CA1-2 and of (spiny) CR-ir neurons in the hilus of the dentate gyrus in transgenic mouse models of AD in vivo, there is evidence in the literature indicating that the pathogenic mechanism of PS1 mutations includes perturbed cellular calcium homeostasis (Mattson and Chan 2003; Smith et al. 2005; Thinakaran and Sisodia 2006). Specifically, PS1 is present at particularly high levels in the endoplasmic reticulum, and cultured neural cells overexpressing mutant forms of PS1 were shown to exhibit increased elevations of cytoplasmic calcium levels when stimulated with agonists that induce calcium release from the endoplasmic reticulum (Mattson and Chan 2003). In fact, mutations in PS1 causing disturbances in the function of low-conductance divalent cation-permeable ion channels in the endoplasmic reticulum formed by PS1 (Tu et al. 2006) as well as in PS1-mediated modulation of the so-called capacitative calcium entry (Yoo et al. 2000), might contribute to increased elevations of cytoplasmic calcium levels following stimulation. A consequence of the enhanced calcium release is that cells expressing mutant PS1 show a lowered excitotoxic threshold for kainic acid in vivo (Schneider et al. 2001), and are more vulnerable to death induced by a variety of stimuli including the exposure to oxidative, metabolic and ischemic insults in vitro (Keller et al. 1998; Mattson and Chan 2003; Mattson et al. 2000). In ischemia, excess activation of ionotropic glutamate receptors also results in increased cytoplasmic calcium levels, followed by cell death (Bano and Nicotera 2007; Orrenius et al. 2003). Recently, Rutten et al. (2005) showed that PS1 overexpression in mice leads to an age-related reduction in synaptophysin-immunoreactive presynaptic boutons in the stratum moleculare. Such reduction in presynaptic terminals was interpreted in this model to be the effect of mutated PS1 and to involve related disruption of cellular calcium homeostasis and calcium signaling, independent of soluble or intraneuronal Aβ (Rutten et al. 2005). Accordingly, we hypothesize that mutations in PS1 may cause a previously unknown selective neuronal vulnerability in the hippocampus, which in itself may contribute to neuronal excitotoxicity in the AD brain by disturbing the inhibition of mossy fibers as outlined above.

It can also be suggested that PS1 initiates the loss of PV-ir and CR-ir neurons by way of its modulation of Aβ processing. It is possible that the PS1 FAD mutations knocked-in in this animal model have an influence on the specificity of the BACE enzyme. Interactions between BACE, PS1, and γ-secretase have been reported (Hattori et al. 2002; Hebert et al. 2003). Moreover, Casas et al. (2004) have demonstrated that APP^{SL}PS1KI mice have altered N-terminal cleavage resulting in the accelerated accumulation of intraneuronal Aβ and intracellular thioflavin S positive material, which can then alter calcium homeostasis and lead to neuronal loss.

It remains to be shown whether other subtypes of hippocampal GABAergic interneurons are involved in this selective vulnerability. In this regard it should be mentioned that in transgenic mice expressing human mutant PS1 (M146L) under control of the HMG promoter (these mice do not show any age-related principal cell loss in the hippocampus; (Schmitz et al. 2004), no age-related reduction in the number of neurons immunoreactive for somatostatin (SOM) and neuropeptide Y (NPY) was found (Ramos et al. 2006; PV- and CR-ir neurons were not investigated in this study). Unfortunately, the analysis of SOM- and NPY-ir neurons was performed on the entire hippocampus in the study by Ramos et al. (2006) rather than in a subregion-specific manner (as in the present study), which may have prevented the detection of age-related, subregion-specific loss of SOM- and NPY-ir neurons.

Age-related neurodegeneration and behavioral abnormalities in APP^{SL}/PS1ho KI mice

Finally, it should be mentioned that APP^{SL}/PS1ho KI mice (but not PS1ho KI mice) are known to show significant working memory and motor task deficits during aging, starting at 6 months of age (Cotel et al. 2008; Wirths et al. 2007). Accordingly, the age-related loss of pyramidal cells in the CA1-2 may contribute at least to the age-related reduction in working memory in the APP^{SL}/PS1ho KI mice, whereas the age-related loss of the PV-ir neurons in the CA1-2 and of the CR-ir neurons in the hilus alone may not be sufficient to cause age-related alterations in working memory (as found for the PS1ho KI mice). However, this should be considered with caution as the APP^{SL}/PS1ho KI mice also showed age-dependent axonal degeneration in other regions of the brain than the hippocampus as well as in the spinal cord (Wirths et al. 2006). Furthermore, the PS1-related selective neuronal vulnerability found in the present study may contribute to age-related disturbances of normal neuronal function observed in mice and rats transgenic for human mutant PS1 (Barrow et al. 2000; Borchardt et al. 1999; Parent et al. 1999; Pybus et al. 2003; Schneider et al. 2001), although this has not yet been investigated in PS1ho KI mice.

In summary, the present study demonstrates a pattern of dissociated, age-related loss of PV- and CR-ir neurons in the hippocampus of a transgenic/knock-in mouse model of AD. This pattern suggests the existence of a previously unknown selective neuronal vulnerability in the hippocampus in AD, which may contribute to excitotoxicity of other neurons in the AD brain. Prevention of the loss of PV- and CR-ir neurons in the hippocampus by maintaining or restoring physiologic calcium homeostasis (see Mattson and Chan 2003; Orrenius et al. 2003) may be relevant in this context, particularly for patients suffering from familial forms of AD involving mutations in PS1.

Acknowledgments

We thank Dr. G. Multhaup for generous gift of antibodies, Drs. V. Blanchard-Bregeon, L. Pradier, and T. Bayer for providing the transgenic animals, and N. Olthof, E. Barth, B. Wicinski, and H.P.J. Steinbusch for expert technical assistance. Supported by grants from the Alzheimer Forschung Initiative e.V., the Internationale Stichting Alzheimer Onderzoek, and NOW 911-06-003 (C.S. and H.W.M.S.), and by NIH grants AG02219 and AG05138 (P.R.H. and D.L.D).

References

Acsady L, Kamondi A, Sik A, Freund T, Buzsaki G. GABAergic cells are the major postsynaptic targets of mossy fibers in the rat hippocampus. J Neurosci 1998;18(9):3386–3403. [PubMed: 9547246]

Arai H, Emson PC, Mountjoy CQ, Carassco LH, Heizmann CW. Loss of parvalbumin-immunoreactive neurones from cortex in Alzheimer-type dementia. Brain Res 1987;418:164–169. [PubMed: 3311290]

Bano D, Nicotera P. Ca2+ signals and neuronal death in brain ischemia. Stroke 2007;38(2 Suppl):674–676. [PubMed: 17261713]

Barrow PA, Empson RM, Gladwell SJ, Anderson CM, Killick R, Yu X, Jefferys JG, Duff K. Functional phenotype in transgenic mice expressing mutant human presenilin-1. Neurobiol Dis 2000;7(2):119–126. [PubMed: 10783295]

Bazzett TJ, Becker JB, Falik RC, Albin RL. Chronic intrastriatal quinolinic acid produces reversible changes in perikaryal calbindin and parvalbumin immunoreactivity. Neuroscience 1994;60(4):837–841. [PubMed: 7523988]

Bonthius DJ, McKim R, Koele L, Harb H, Karacay B, Mahoney J, Pantazis NJ. Use of frozen sections to determine neuronal number in the murine hippocampus and neocortex using the optical dissector and optical fractionator. Brain Res Brain Res Protoc 2004;14(1):45–57. [PubMed: 15519951]

Borchardt T, Camakaris J, Cappai R, Masters CL, Beyreuther K, Multhaup G. Copper inhibits beta-amyloid production and stimulates the non-amyloidogenic pathway of amyloid-precursor-protein secretion. Biochem J 1999;344(Pt 2):461–467. [PubMed: 10567229]

Braak H, Braak E. Neuropathological staging of Alzheimer-related changes. Acta Neuropathol 1991;82(4):239–259. [PubMed: 1759558]

Brady DR, Mufson EJ. Parvalbumin-immunoreactive neurons in the hippocampal formation of Alzheimer's diseased brain. Neuroscience 1997;80(4):1113–1125. [PubMed: 9284064]

Brion JP, Résibois A. A subset of calretinin-positive neurons are abnormal in Alzheimer's disease. Acta Neuropathol 1994;88(1):33–43. [PubMed: 7941970]

Calhoun ME, Wiederhold KH, Abramowski D, Phinney AL, Probst A, Sturchler-Pierrat C, Staufenbiel M, Sommer B, Jucker M. Neuron loss in APP transgenic mice. Nature 1998;395(6704):755–756. [PubMed: 9796810]

Casas C, Sergeant N, Itier JM, Blanchard V, Wirths O, van der Kolk N, Vingtdeux V, van de Steeg E, Ret G, Canton T, Drobecq H, Clark A, Bonici B, Delacourte A, Benavides J, Schmitz C, Tremp G, Bayer TA, Benoit P, Pradier L. Massive CA1/2 neuronal loss with intraneuronal and N-terminal truncated Abeta42 accumulation in a novel Alzheimer transgenic model. Am J Pathol 2004;165(4):1289–1300. [PubMed: 15466394]

Cotel MC, Bayer TA, Wirths O. Age-dependent loss of dentate gyrus granule cells in APP/PS1KI mice. Brain Res 2008;1222:207–213. [PubMed: 18585693]

Cummings JL, Cole G. Alzheimer disease. JAMA 2002;287(18):2335–2338. [PubMed: 11988038]

Dickson DW. Building a more perfect beast: APP transgenic mice with neuronal loss. Am J Pathol 2004;164(4):1143–1146. [PubMed: 15039203]

Dominguez MI, Blasco-Ibanez JM, Crespo C, Marques-Mari AI, Martinez-Guijarro FJ. Calretinin/PSA-NCAM immunoreactive granule cells after hippocampal damage produced by kainic acid and DEDTC treatment in mouse. Brain Res 2003;966(2):206–217. [PubMed: 12618344]

Ferrer I, Soriano E, Tunon T, Fonseca M, Guionnet N. Parvalbumin immunoreactive neurons in normal human temporal neocortex and in patients with Alzheimer's disease. J Neurol Sci 1991;106:135–141. [PubMed: 1802961]

Ferrer I, Tunon T, Serrano MT, Casas R, Alcantara S, Zujar MJ, Rivera RM. Calbindin D-28k and parvalbumin immunoreactivity in the frontal cortex in patients with frontal lobe dementia of non Alzheimer type associated with amyotrophic lateral sclerosis. J Neurol Neurosurg Psychiatry 1993a;56:257–261. [PubMed: 8459241]

Ferrer I, Zujar MJ, Rivera R, Soria M, Vidal A, Casas R. Parvalbumin-immunoreactive dystrophic neurites and aberrant sprouts in the cerebral cortex of patients with Alzheimer's disease. Neurosci Lett 1993b;158:163–166. [PubMed: 8233090]

Fonseca M, Soriano E, Ferrer I, Martinez A, Tunon T. Chandelier cell axons identified by parvalbumin-immunoreactivity in the normal human temporal cortex and in Alzheimer's disease. Neuroscience 1993;55:1107–1116. [PubMed: 8232900]

Franklin, KBJ.; Paxinos, G. The mouse brain in stereotaxic coordinates. Academic Press; San Diego: 1997.

Freund TF, Buzsaki G. Interneurons of the hippocampus. Hippocampus 1996;6(4):347–470. [PubMed: 8915675]

Freund TF, Magloczky Z. Early degeneration of calretinin-containing neurons in the rat hippocampus after ischemia. Neuroscience 1993;56(3):581–596. [PubMed: 8255422]

Fuchs EC, Zivkovic AR, Cunningham MO, Middleton S, Lebeau FE, Bannerman DM, Rozov A, Whittington MA, Traub RD, Rawlins JN, Monyer H. Recruitment of parvalbumin-positive interneurons determines hippocampal function and associated behavior. Neuron 2007;53(4):591–604. [PubMed: 17296559]

Gsell W, Jungkunz G, Riederer P. Functional neurochemistry of Alzheimer's disease. Curr Pharm Des 2004;10(3):265–293. [PubMed: 14754387]

Gulyas AI, Hajos N, Freund TF. Interneurons containing calretinin are specialized to control other interneurons in the rat hippocampus. J Neurosci 1996;16(10):3397–3411. [PubMed: 8627375]

Hattori C, Asai M, Oma Y, Kino Y, Sasagawa N, Saido TC, Maruyama K, Ishiura S. BACE1 interacts with nicastrin. Biochem Biophys Res Commun 2002;293(4):1228–1232. [PubMed: 12054507]

Hebert SS, Bourdages V, Godin C, Ferland M, Carreau M, Levesque G. Presenilin-1 interacts directly with the beta-site amyloid protein precursor cleaving enzyme (BACE1). Neurobiol Dis 2003;13(3):238–245. [PubMed: 12901838]

Hof PR, Morrison JH. Neocortical neuronal subpopulations labeled by a monoclonal antibody to calbindin exhibit differential vulnerability in Alzheimer's disease. Exp Neurol 1991;111:293–301. [PubMed: 1999232]

Hof PR, Morrison JH. The aging brain: morphomolecular senescence of cortical circuits. Trends Neurosci 2004;27(10):607–613. [PubMed: 15374672]

Hof PR, Cox K, Young WG, Celio MR, Rogers J, Morrison JH. Parvalbumin-immunoreactive neurons in the neocortex are resistant to degeneration in Alzheimer's disease. J Neuropathol Exp Neurol 1991;50(4):451–462. [PubMed: 2061713]

Hof PR, Nimchinsky EA, Celio MR, Bouras C, Morrison JH. Calretinin-immunoreactive neocortical interneurons are unaffected in Alzheimer's disease. Neurosci Lett 1993;152(1–2):145–148. [PubMed: 8515868]

Howlett DR, Bowler K, Soden PE, Riddell D, Davis JB, Richardson JC, Burbidge SA, Gonzalez MI, Irving EA, Lawman A, Miglio G, Dawson EL, Howlett ER, Hussain I. Abeta deposition and related pathology in an APP × PS1 transgenic mouse model of Alzheimer's disease. Histol Histopathol 2008;23(1):67–76. [PubMed: 17952859]

Inaguma Y, Shinohara H, Inagaki T, Kato K. Immunoreactive parvalbumin concentrations in parahippocampal gyrus decrease in patients with Alzheimer's disease. J Neurol Sci 1992;110:57–61. [PubMed: 1506869]

Irizarry MC, Soriano F, McNamara M, Page KJ, Schenk D, Games D, Hyman BT. Abeta deposition is associated with neuropil changes, but not with overt neuronal loss in the human amyloid precursor protein V717F (PDAPP) transgenic mouse. J Neurosci 1997;17(18):7053–7059. [PubMed: 9278541]

Kaufmann WA, Barnas U, Humpel C, Nowakowski K, De Col C, Gurka P, Ransmayr G, Hinterhuber H, Winkler H, Marksteiner J. Synaptic loss reflected by secretoneurin-like immunoreactivity in the human hippocampus in Alzheimer's disease. Eur J Neurosci 1998;10(3):1084–1094. [PubMed: 9753176]

Keller JN, Guo Q, Holtsberg FW, Bruce-Keller AJ, Mattson MP. Increased sensitivity to mitochondrial toxin-induced apoptosis in neural cells expressing mutant presenilin-1 is linked to perturbed calcium homeostasis and enhanced oxyradical production. J Neurosci 1998;18(12):4439–4450. [PubMed: 9614221]

Lanctot KL, Herrmann N, Mazzotta P, Khan LR, Ingber N. GABAergic function in Alzheimer's disease: evidence for dysfunction and potential as a therapeutic target for the treatment of

behavioural and psychological symptoms of dementia. Can J Psychiatry 2004;49(7):439–453. [PubMed: 15362248]

Lazarov O, Peterson LD, Peterson DA, Sisodia SS. Expression of a familial Alzheimer's disease-linked presenilin-1 variant enhances perforant pathway lesion-induced neuronal loss in the entorhinal cortex. J Neurosci 2006;26(2):429–434. [PubMed: 16407539]

Lee KW, Lee SH, Kim H, Song JS, Yang SD, Paik SG, Han PL. Progressive cognitive impairment and anxiety induction in the absence of plaque deposition in C57BL/6 inbred mice expressing transgenic amyloid precursor protein. J Neurosci Res 2004;76(4):572–580. [PubMed: 15114629]

Leuba G, Kraftsik R, Saini K. Quantitative distribution of parvalbumin, calretinin, and calbindin D-28k immunoreactive neurons in the visual cortex of normal and Alzheimer cases. Exp Neurol 1998;152:278–291. [PubMed: 9710527]

Maccaferri G, Lacaille JC. Interneuron diversity series: hippocampal interneuron classifications—making things as simple as possible, not simpler. Trends Neurosci 2003;26(10):564–571. [PubMed: 14522150]

Mattson MP, Chan SL. Neuronal and glial calcium signaling in Alzheimer's disease. Cell Calcium 2003;34(4–5):385–397. [PubMed: 12909083]

Mattson MP, Zhu H, Yu J, Kindy MS. Presenilin-1 mutation increases neuronal vulnerability to focal ischemia in vivo and to hypoxia and glucose deprivation in cell culture: involvement of perturbed calcium homeostasis. J Neurosci 2000;20(4):1358–1364. [PubMed: 10662826]

Mikkonen M, Alafuzoff I, Tapiola T, Soininen H, Miettinen R. Subfield- and layer-specific changes in parvalbumin, calretinin and calbindin-D28K immunoreactivity in the entorhinal cortex in Alzheimer's disease. Neuroscience 1999;92:515–532. [PubMed: 10408601]

Moga DE, Janssen WG, Vissavajjhala P, Czelusniak SM, Moran TM, Hof PR, Morrison JH. Glutamate receptor subunit 3 (GluR3) immunoreactivity delineates a subpopulation of parvalbumin-containing interneurons in the rat hippocampus. J Comp Neurol 2003;462(1):15–28. [PubMed: 12761821]

Morris JC. The clinical dementia rating (CDR): current version and scoring rules. Neurology 1993;43(11):2412–2414. [PubMed: 8232972]

Nimchinsky EA, Vogt BA, Morrison JH, Hof PR. Neurofilament and calcium-binding proteins in the human cingulate cortex. J Comp Neurol 1997;384(4):597–620. [PubMed: 9259492]

Nomura T, Fukuda T, Aika Y, Heizmann CW, Emson PC, Kobayashi T, Kosaka T. Distribution of nonprincipal neurons in the rat hippocampus, with special reference to their dorsoventral difference. Brain Res 1997;751(1):64–80. [PubMed: 9098569]

Orrenius S, Zhivotovsky B, Nicotera P. Regulation of cell death: the calcium–apoptosis link. Nat Rev Mol Cell Biol 2003;4(7):552–565. [PubMed: 12838338]

Palop JJ, Jones B, Kekonius L, Chin J, Yu GQ, Raber J, Masliah E, Mucke L. Neuronal depletion of calcium-dependent proteins in the dentate gyrus is tightly linked to Alzheimer's disease-related cognitive deficits. Proc Natl Acad Sci USA 2003;100(16):9572–9577. [PubMed: 12881482]

Parent A, Linden DJ, Sisodia SS, Borchelt DR. Synaptic transmission and hippocampal long-term potentiation in transgenic mice expressing FAD-linked presenilin 1. Neurobiol Dis 1999;6(1):56–62. [PubMed: 10078973]

Popovic M, Caballero-Bleda M, Kadish I, Van Groen T. Subfield and layer-specific depletion in calbindin-D28K, calretinin and parvalbumin immunoreactivity in the dentate gyrus of amyloid precursor protein/presenilin 1 transgenic mice. Neuroscience 2008;155(1):182–191. [PubMed: 18583063]

Pybus R, Barnard E, Estibeiro P, Mullins J, MacLeod N. Enhanced long-term potentiation in the hippocampus of rats expressing mutant presenillin-1 is age related. Neurobiol Dis 2003;12(3):212–224. [PubMed: 12742741]

Ramos B, Baglietto-Vargas D, del Rio JC, Moreno-Gonzalez I, Santa-Maria C, Jimenez S, Caballero C, Lopez-Tellez JF, Khan ZU, Ruano D, Gutierrez A, Vitorica J. Early neuropathology of somatostatin/NPY GABAergic cells in the hippocampus of a PS1 × APP transgenic model of Alzheimer's disease. Neurobiol Aging 2006;27(11):1658–1672. [PubMed: 16271420]

Rutten BP, Wirths O, Van de Berg WD, Lichtenthaler SF, Vehoff J, Steinbusch HW, Korr H, Beyreuther K, Multhaup G, Bayer TA, Schmitz C. No alterations of hippocampal neuronal number

and synaptic bouton number in a transgenic mouse model expressing the beta-cleaved C-terminal APP fragment. Neurobiol Dis 2003;12(2):110–120. [PubMed: 12667466]

Rutten BP, Van der Kolk NM, Schafer S, van Zandvoort MA, Bayer TA, Steinbusch HW, Schmitz C. Age-related loss of synaptophysin immunoreactive presynaptic boutons within the hippocampus of APP751SL, PS1M146L, and APP751SL/PS1M146L transgenic mice. Am J Pathol 2005;167(1): 161–173. [PubMed: 15972962]

Satoh J, Tabira T, Sano M, Nakayama H, Tateishi J. Parvalbumin-immunoreactive neurons in the human central nervous system are decreased in Alzheimer's disease. Acta Neuropathol 1991;81:388–395. [PubMed: 2028743]

Schmidt ML, Robinson KA, Lee VM, Trojanowski JQ. Chemical and immunological heterogeneity of fibrillar amyloid in plaques of Alzheimer's disease and Down's syndrome brains revealed by confocal microscopy. Am J Pathol 1995;147(2):503–515. [PubMed: 7639340]

Schmitz C, Hof PR. Design-based stereology in neuroscience. Neuroscience 2005;130:813–831. [PubMed: 15652981]

Schmitz C, Rutten BP, Pielen A, Schafer S, Wirths O, Tremp G, Czech C, Blanchard V, Multhaup G, Rezaie P, Korr H, Steinbusch HW, Pradier L, Bayer TA. Hippocampal neuron loss exceeds amyloid plaque load in a transgenic mouse model of Alzheimer's disease. Am J Pathol 2004;164(4):1495–1502. [PubMed: 15039236]

Schneider I, Reverse D, Dewachter I, Ris L, Caluwaerts N, Kuiperi C, Gilis M, Geerts H, Kretzschmar H, Godaux E, Moechars D, Van Leuven F, Herms J. Mutant presenilins disturb neuronal calcium homeostasis in the brain of transgenic mice, decreasing the threshold for excitotoxicity and facilitating long-term potentiation. J Biol Chem 2001;276(15):11539–11544. [PubMed: 11278803]

Schwaller B, Buchwald P, Blumcke I, Celio MR, Hunziker W. Characterization of a polyclonal antiserum against the purified human recombinant calcium binding protein calretinin. Cell Calcium 1993;14(9):639–648. [PubMed: 8242719]

Scotti AL, Kalt G, Bollag O, Nitsch C. Parvalbumin disappears from GABAergic CA1 neurons of the gerbil hippocampus with seizure onset while its presence persists in the perforant path. Brain Res 1997;760(1–2):109–117. [PubMed: 9237525]

Selke K, Muller A, Kukley M, Schramm J, Dietrich D. Firing pattern and calbindin-D28k content of human epileptic granule cells. Brain Res 2006;1120(1):191–201. [PubMed: 16997289]

Shu SY, Ju G, Fan LZ. The glucose oxidase-DAB-nickel method in peroxidase histochemistry of the nervous system. Neurosci Lett 1988;85(2):169–171. [PubMed: 3374833]

Smith IF, Green KN, La Ferla FM. Calcium dysregulation in Alzheimer's disease: recent advances gained from genetically modified animals. Cell Calcium 2005;38(3–4):427–437. [PubMed: 16125228]

Solodkin A, Veldhuizen SD, Van Hoesen GW. Contingent vulnerability of entorhinal parvalbumin-containing neurons in Alzheimer's disease. J Neurosci 1996;16:3311–3321. [PubMed: 8627368]

Takeuchi A, Irizarry MC, Duff K, Saido TC, Hsiao Ashe K, Hasegawa M, Mann DM, Hyman BT, Iwatsubo T. Age-related amyloid beta deposition in transgenic mice overexpressing both Alzheimer mutant presenilin 1 and amyloid beta precursor protein Swedish mutant is not associated with global neuronal loss. Am J Pathol 2000;157(1):331–339. [PubMed: 10880403]

Thinakaran G, Sisodia SS. Presenilins and Alzheimer disease: the calcium conspiracy. Nat Neurosci 2006;9(11):1354–1355. [PubMed: 17066063]

Tu H, Nelson O, Bezprozvanny A, Wang Z, Lee SF, Hao YH, Serneels L, De Strooper B, Yu G, Bezprozvanny I. Presenilins form ER Ca2+ leak channels, a function disrupted by familial Alzheimer's disease-linked mutations. Cell 2006;126(5):981–993. [PubMed: 16959576]

Van Broeck B, Vanhoutte G, Pirici D, Van Dam D, Wils H, Cuijt I, Vennekens K, Zabielski M, Michalik A, Theuns J, De Deyn PP, Van der Linden A, Van Broeckhoven C, Kumar-Singh S. Intraneuronal amyloid beta and reduced brain volume in a novel APP T714I mouse model for Alzheimer's disease. Neurobiol Aging 2008;29(2):241–252. [PubMed: 17112635]

Van Der Gucht E, Youakim M, Arckens L, Hof PR, Baizer JS. Variations in the structure of the prelunate gyrus in Old World monkeys. Anat Rec A Discov Mol Cell Evol Biol 2006;288(7):753–775. [PubMed: 16779809]

West MJ, Coleman PD, Flood DG, Troncoso JC. Differences in the pattern of hippocampal neuronal loss in normal ageing and Alzheimer's disease. Lancet 1994;344(8925):769–772. [PubMed: 7916070]

Wirths O, Multhaup G, Czech C, Feldmann N, Blanchard V, Tremp G, Beyreuther K, Pradier L, Bayer TA. Intraneuronal APP/A beta trafficking and plaque formation in beta-amyloid precursor protein and presenilin-1 transgenic mice. Brain Pathol 2002;12:275–286. [PubMed: 12146796]

Wirths O, Weis J, Szczygielski J, Multhaup G, Bayer TA. Axonopathy in an APP/PS1 transgenic mouse model of Alzheimer's disease. Acta Neuropathol 2006;111(4):312–319. [PubMed: 16520967]

Wirths O, Weis J, Kayed R, Saido TC, Bayer TA. Age-dependent axonal degeneration in an Alzheimer mouse model. Neurobiol Aging 2007;28(11):1689–1699. [PubMed: 16963164]

Yoo AS, Cheng I, Chung S, Grenfell TZ, Lee H, Pack-Chung E, Handler M, Shen J, Xia W, Tesco G, Saunders AJ, Ding K, Frosch MP, Tanzi RE, Kim TW. Presenilin-mediated modulation of capacitative calcium entry. Neuron 2000;27(3):561–572. [PubMed: 11055438]

Zhang ZJ, Reynolds GP. A selective decrease in the relative density of parvalbumin-immunoreactive neurons in the hippocampus in schizophrenia. Schizophr Res 2002;55:1–10. [PubMed: 11955958]

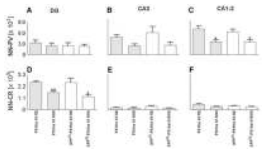

Fig. 1.

Mean and standard error of the mean (SEM) of estimated numbers of PV-ir neurons (**a–c**; NN-PV) and numbers of CR-ir neurons (**d–f**; NN-CR) in the dentate gyrus and hilus (DG; **a**, **d**), CA3 (**b**, **e**), and CA1-2 (stratum pyramidale) (**c**, **f**) in the hippocampus of either 2-month-old (M2) or 10-month-old (M10) PS1ho KI mice (*light gray bars*) and APP^{SL}/PS1ho KI mice (*open bars*). Results of general linear model univariate analysis of variance are summarized in Table 2; results of post hoc Bonferroni tests for pairwise comparisons between animals in groups M2 and M10, of the same genotype are indicated in the graphs. $*p < 0.05$, $**p < 0.01$

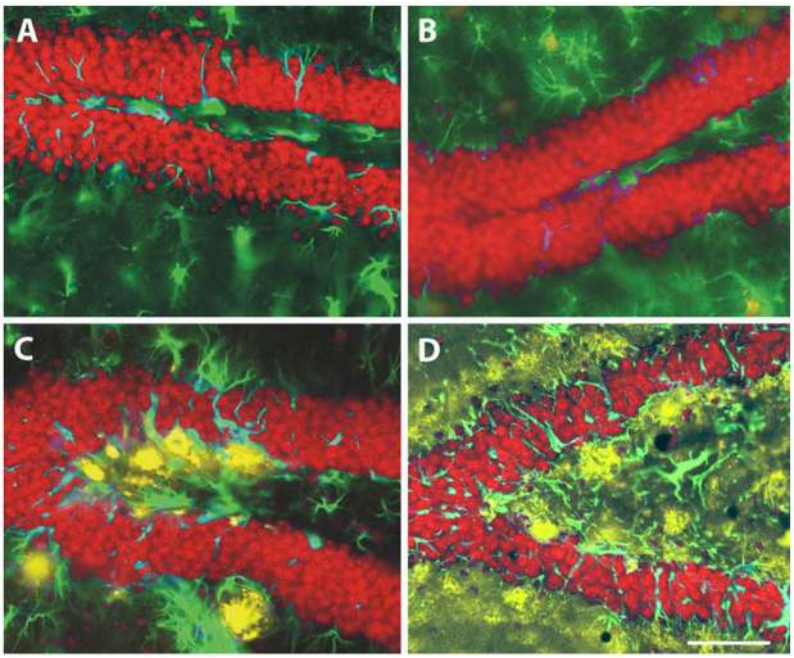

Fig. 2.

Representative high-power photomicrographs showing region-specific immunofluorescence detection of A*β* (*yellow fluorescence*) and GFAP (*green fluorescence*) within the dentate gyrus in the hippocampus of APP^{SL} mice at 2 month of age (M2; **a**) and 10 months of age (M10; **c**) as well as of APP^{SL}/PS1ho KI mice at M2 (**b**) and M10 (**d**) (sections counterstained with Hoechst 33342, pseudocolored in *red* for better contrast). Note the age-related aggregation of extracellular Aβ, the strong increase in GFAP immunoreactivity and particularly the neuron loss in the APP^{SL}/PS1ho KI mice. *Scale bar* 33 μm

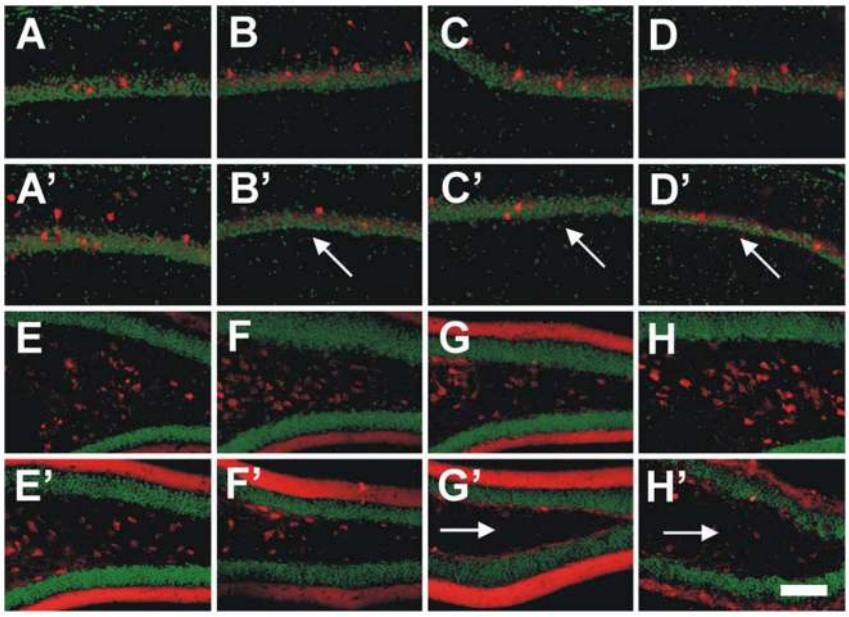

Fig. 3.

Immunohistochemical detection of parvalbumin (PV) in the area CA1-2 (*red fluorescence* in **a**–**d** and **a′**–**d′**) and calretinin (CR) in the DG (*red fluorescence* in **e**–**h** and **e′**–**h′**) in the hippocampus of 2-month-old (**a**–**h**) and 10-month-old (**a′**–**h′**) APP^{SL} mice (**a**, **a′**, **e**, **e′**), PS1he KI mice (**b**, **b′**, **f**, **f′**), PS1ho KI mice (**c**, **c′**, **g**, **g′**) and APP^{SL}/PS1ho KI mice (**d**, **d′**, **h**, **h′**). Sections were counterstained with Hoechst (pseudocolored in *green* for better contrast). Note the substantial age-related loss of PV-ir neurons in the CA1-2 of the PS1he KI mice, PS1ho KI mice and APP^{SL}/PS1ho KI mice (*arrows* in **b′**, **c′** and **d′**), as well as of CR-ir neurons in the dentate gyrus and hilus of the PS1ho KI mice and APP^{SL}/PS1ho KI mice (*arrows* in **g′** and **h′**). *Scale bar* 100 μm

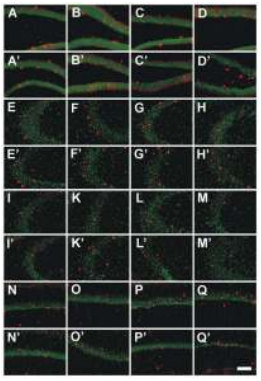

Fig. 4.

Immunohistochemical detection of parvalbumin (PV) (*red fluorescence* in **a–h** and **a′**–**h′**) and calretinin (CR) (*red fluorescence* in **i–q** and **i′**–**q′**) within the DG (**a**–**d′**), the CA3 (**e**–**m′**) and the CA1-2 (**n**–**q′**) regions of the hippocampus of 2-month-old (**a–h** and **i–q**) and 10-month-old (**a′**–**h′** and **i′**–**q′**) APP^{SL} mice (**a**, **a′**, **e**, **e′**, **i**, **i′**, **n**, **n′**), PS1he KI mice (**b**, **b′**, **f**, **f′**, **k**, **k′**, **o**, **o′**), PS1ho KI mice (**c**, **c′**, **g**, **g′**, **l**, **l′**, **p**, **p′**) and APP^{SL}/PS1ho KI mice (**d**, **d′**, **h**, **h′**, **m**, **m′**, **q**, **q′**). Sections were counterstained with Hoechst (pseudocolored in *green* for better contrast). *Scale bar* 100 μm

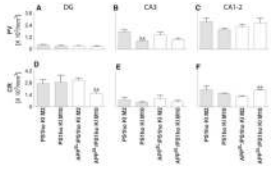

Fig. 5.

Densities of PV-ir neurons (**a–c**) and CR-ir neurons (**d–f**) (means ± SEM) in the dentate gyrus (DG; **a, d**), CA3 (**b, e**), and CA1-2 (**c, f**) in the hippocampus of 2-month-old (M2) and 10-month-old (M10) PS1ho KI mice (*light gray bars*) and APP^{SL}/PS1ho KI mice (*open bars*). Results of general linear model univariate analysis of variance are summarized in Table 2; results of post hoc Bonferroni tests for pairwise comparisons between animals in groups M2 and M10 of the same genotype are indicated in the graphs.
$^{**}p < 0.01$

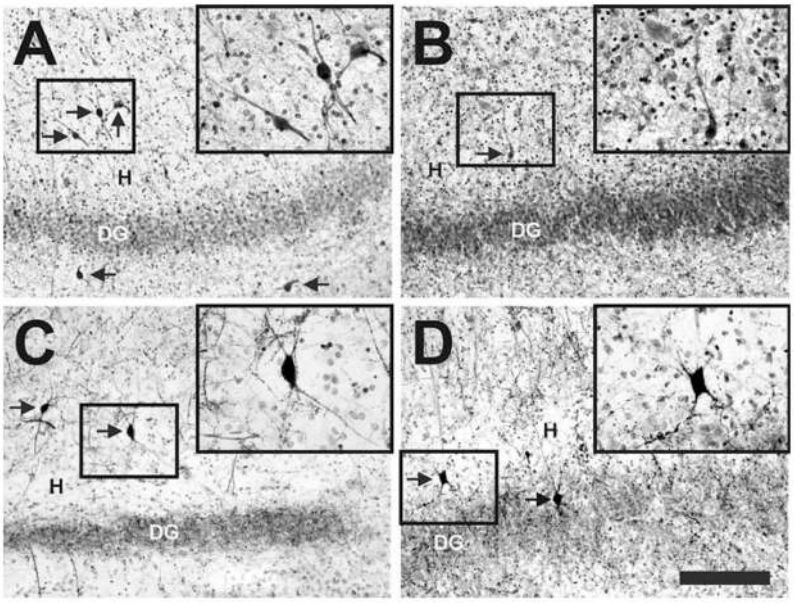

Fig. 6.

Representative photomicrographs of sections from human postmortem brains of a control (**a, c**) and an AD patient (**b, d**) showing neurons immunoreactive for CR (**a, b**) and PV (**c, d**) (*arrows*) within the dentate gyrus (*DG*) and hilus (*H*) of the hippocampus. The *rectangles* show the positions at which the high-power photomicrographs (*insets*) were taken. Note the loss of CR-immunoreactive neurons in the brain from the AD patient and the substantial gliosis within the hilus of this brain (*inset* in **b**). *Scale bar* 200 μm (50 μm for the *insets*)

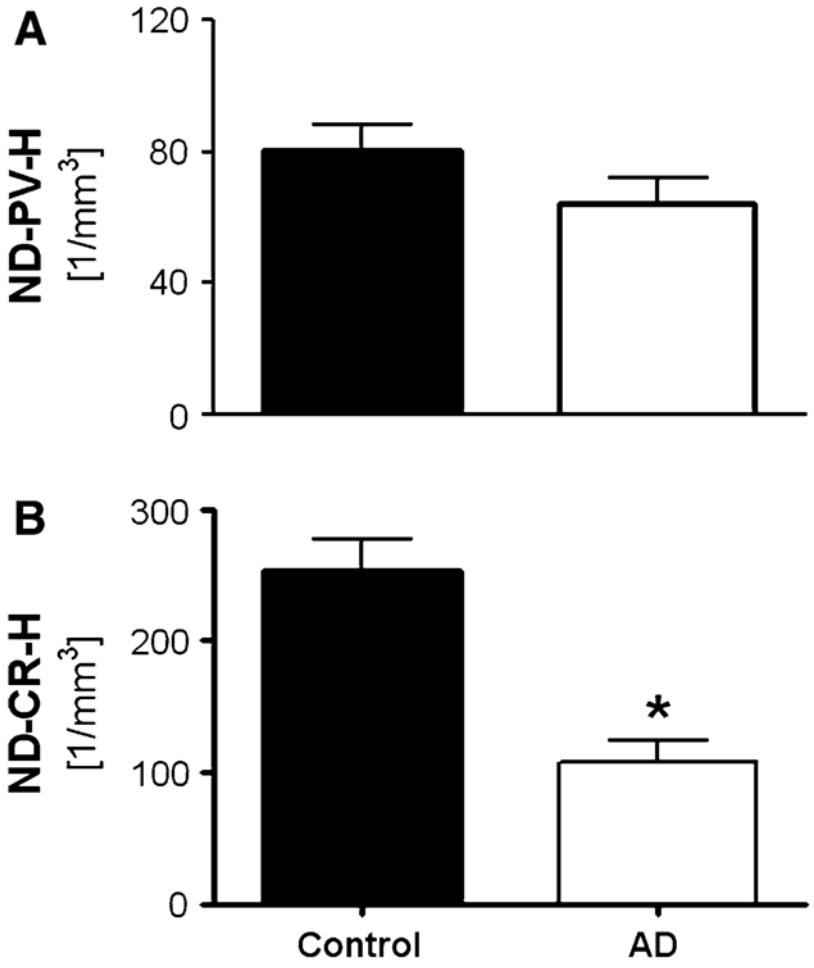

Fig. 7.

Mean and standard error of the mean (SEM) of densities of PV-ir neurons (**a**; ND-PV-H) or CR-ir neurons (**b**; ND-CR-H) in the dentate gyrus and hilus in postmortem brains from either control subjects (*black bars*) or AD subjects (*open bars*). Results of general linear model univariate analysis of variance are summarized in Table 2 and indicated in the graph. *p <0.01

Table 1

Characteristics of human cases used in this study

Case	Gender	Age	Diagnosis	Braak and Braak neurofibrillary staging	CDR
1	M	85	Control	1	0
2	M	98	Control	3	0
3	M	85	Control	3	0.5
4	M	74	Control	1	0
5	M	82	Control	1	0.5
6	W	94	Control	3	0.5
7	W	79	Control	1	0
8	W	69	Control	1	0.5
9	W	89	Control	2	0
10	W	91	Control	1	0.5
11	W	85	AD	5	5
12	W	94	AD	6	5
13	W	88	AD	3	3
14	W	83	AD	5	5
15	W	95	AD	6	3
16	M	90	AD	6	3
17	M	88	AD	3	3
18	M	85	AD	5	5
19	M	86	AD	5	4
20	M	70	AD	4	3

AD Alzheimer's disease, *CDR* clinical dementia rating score (Morris 1993), *M* man, *W* woman

Table 2

Results (p values) of general linear model univariate analysis of variance

Variable	Region	*E/R*	P_{gender}	P_{age}	$P_{genotype}/P_{diagnosis}$	$P_{age \times genotype}$
V	DG		**0.040**	**0.036**	0.204	0.398
	CA3		0.715	**0.021**	**0.011**	0.085
	CA1-2		0.950	**<0.001**	0.984	**0.032**
	WM		0.861	0.339	0.816	0.499
NN-PV	DG	E	0.278	0.785	0.786	0.288
		R	0.289	0.854	0.827	0.282
	CA3	E	0.505	**0.011**	0.701	0.143
		R	0.530	**0.014**	0.660	0.170
	CA1-2	E	0.086	**<0.001**	0.306	**0.037**
		R	0.088	**<0.001**	0.284	**0.037**
	WM	E	**0.030**	0.849	**0.014**	**0.008**
		R	**0.031**	0.669	**0.012**	**0.007**
NN-CR	DG	E	0.139	**0.002**	0.700	0.119
		R	0.148	**0.003**	0.675	0.143
	CA3	E	0.491	**0.024**	0.226	0.258
		R	0.466	**0.024**	0.171	0.299
	CA1-2	E	0.490	0.066	**0.007**	0.224
		R	0.491	0.067	**0.006**	0.153
	WM	E	**0.045**	0.151	**0.006**	0.798
		R	**0.022**	0.262	**0.005**	0.720
ND-PV	DG		0.337	0.842	0.339	0.370
	CA3		0.341	0.106	0.077	0.327
	CA1-2		0.071	0.716	0.130	0.063
	WM		0.080	0.550	**0.044**	0.052
ND-CR	DG		0.242	0.189	0.376	0.281
	CA3		0.229	0.076	0.347	0.216
	CA1-2		0.259	0.164	**0.006**	0.076
	WM		0.066	0.901	0.062	0.810
ND-PV-H	DG		0.723	0.811	0.435	

Variable	Region	*E/R*	P_{gender}	P_{age}	$P_{genotype}/P_{diagnosis}$	$P_{age \times genotype}$
ND-CR–H	DG		0.921	0.106	**0.001**	

P values smaller than 0.05 are shown in boldface

V volume, *NN-PV* number of parvalbumin-ir neurons, *NN-CR* number of calretinin-ir neurons, *ND-PV* density of PV-ir neurons, *ND-CR* density of CR-ir neurons, *ND-PV-H* density of PV-ir neurons in the human brain, *ND-CR–H* density of CR-ir neurons in the human brain, *DG* dentate gyrus (stratum granulare and hilus), *CA1-2* area CA1-2 (stratum pyramidale), *CA3* area CA3 (stratum pyramidale), *WM* white matter, *E* estimated neuron numbers, *R* reconstructed neuron numbers, taking local amounts of extracellular Aβ aggregation into account (see “Materials and methods” and Casas et al. 2004)

Table 3

Summary of data on PV and CR expression in neuronal subpopulations

Region	Tissue source	Marker	Outcome
CA1-2-SP	APP^{SL} mice	PV	No difference in the number of PV-ir neurons with age
	PS1he KI mice	PV	43.8% reduction in number of PV-ir neurons with age
	PS1ho KI mice	PV	49.4% reduction in number of PV-ir neurons with age
	APP^{SL}/PS1ho KI mice	PV	42.7% reduction in number of PV-ir neurons with age
DG-SG and hilus	PS1ho KI mice	CR	37.8% reduction in number of CR-ir neurons with age
	APP^{SL}/PS1ho KI mice	CR	51.6% reduction in number of CR-ir neurons with age; 49.3% reduction in density of CR-ir neurons with age
	Human AD brains	PV	PV-ir neurons distributed within or close to the stratum granulare; no change in density from AD cases compared to controls
	Human AD brains	CR	CR-ir neurons mainly distributed in the hilar region of the dentate gyrus; 63.2% reduction in the densities of CR-ir neurons from AD cases compared to controls

DG-SG dentate gyrus-stratum granulare and hilus, *CA1-2* area CA1-2 (stratum pyramidale), *PV* parvalbumin, *CR* calretinin

Table 4

Summary of published reports on calcium-binding protein-expressing/GABAergic neuronal subpopulations in AD

Reference	Regions	Markers	Outcome
Fonseca et al. (1993)	TC	PV	PV chandelier cells modified, accompanied with dystrophic neurites and sprouting
Mikkonen et al. (1999)	EC	PV, CR, CB	PV and CB reduced
Solodkin et al. (1996)	EC	PV	Reduced
Brady and Mufson (1997)	Hi	PV	Reduced (DG/CA4, CA1-2)
Ferrer et al. (1993a)	FC	PV, CB	CB reduced
Arai et al. (1987)	FC, TC	PV	Reduced numbers and size
Satoh et al. (1991)	FC, PC, OC	PV	Reduced (parahippocampal gyrus)
Inaguma et al. (1992)	FC, PC, OC	PV	Reduced (parahippocampal gyrus),
Brion and Résibois (1994)	Hi	CR	Dystrophic neurites (parahippocampal gyrus and subiculum)
Kaufmann et al. (1998)	Hi	CR	Reduced (innermost part of the molecular layer)
Leuba et al. (1998)	VC	PV, CR, CB	Preserved
Ferrer et al. (1993b)	TC	PV	Preserved
Hof and Morrison (1991)	FC	CB	Preserved
Ferrer et al. (1991)	TC	PV	Preserved
Hof et al. (1991)	PFC, ITC	PV	Preserved
Fonseca and Soriano (1995)	TC	CR	Preserved
Hof et al. (1993)	PFC, ITC	CR	Preserved
Popovic et al. (2008)	Hi	PV, CR, CB	Reduced

TC temporal cortex, *EC* entorhinal cortex, *Hi* hippocampus, *FC* frontal cortex, *PC* parietal cortex, *OC* occipital cortex, *VC* visual cortex, *PFC* prefrontal cortex, *ITC* inferior temporal cortex, *PV* parvalbumin, *CR* calretinin, *CB* calbindin